Li, X., Zhang, K., Zhang, Q., Zhang, W., Yuan, Y., Li, X. (2018): Integrated Orbit Determination of FengYun-3C, BDS, and GPS Satellites. - *Journal of Geophysical Research*, *123*, 9, pp. 8143—8160.

DOI: http://doi.org/10.1029/2018JB015481

Journal of Geophysical Research: Solid Earth

RESEARCH ARTICLE
10.1029/2018JB015481

Key Points:
- We develop an integrated orbit determination of FY-3C, BDS, and GPS satellites
- The result shows that the integrated orbit determination can significantly improve the orbit of both FY-3C and navigation satellites
- The SLR validation results further confirm the benefit of integrated orbit determination

Correspondence to:
X. Li,
lxlq109121@gmail.com

Citation:
Li, X., Zhang, K., Zhang, Q., Zhang, W., Yuan, Y., & Li, X. (2018). Integrated orbit determination of FengYun-3C, BDS, and GPS satellites. *Journal of Geophysical Research: Solid Earth*, *123*, 8143–8160. https://doi.org/10.1029/2018JB015481

Received 12 JAN 2018
Accepted 19 AUG 2018
Accepted article online 28 AUG 2018
Published online 15 SEP 2018

Integrated Orbit Determination of FengYun-3C, BDS, and GPS Satellites

Xingxing Li[1,2], Keke Zhang[1], Qian Zhang[1], Wei Zhang[1], Yongqiang Yuan[1], and Xin Li[1]

[1]School of Geodesy and Geomatics, Wuhan University, Wuhan, China, [2]German Research Centre for Geosciences (GFZ), Potsdam, Germany

Abstract Aiming at weather forecast and global climate research, the satellite FengYun-3C (FY-3C), as the new generation of China's weather satellites, was launched in 2013. It carries the Global Navigation Satellite Systems Occultation Sounder instrument, a BDS + GPS receiver, to fulfill the demand of orbit determination and occultation. In this contribution, we develop an integrated orbit determination of FY-3C, BDS, and GPS satellites by joint processing of onboard FY-3C and ground data during 2013–2017. Four processing schemes, BDS, GPS, BDS + GPS, and BDS (without Geostationary Earth Orbit [GEO]) + GPS, are designed to investigate the capability of BDS for the integrated precise orbit determination and the benefit of BDS and GPS fusion. Regional and global networks are also employed to analyze the influence of station distribution on the orbit determination. The results show that with a regional network, both BDS and GPS orbits present a significant improvement after including FY-3C data. For the BDS + GPS one-step solution, GPS orbits are improved by 20% compared with the two-step solution, while the improvement can reach 42%, 27%, and 27% for BDS GEO, Inclined Geosynchronous Satellite Orbit, and Medium Earth Orbit, respectively. The precision improvement of FY-3C is respectively 26%, 44%, and 30% in along, cross, and radial components. For a global network, the orbit precision of the BDS + GPS solution is improved by 4% for GPS and 5%, 16%, and 19% for BDS GEO, Inclined Geosynchronous Satellite Orbit, and Medium Earth Orbit, respectively. For FY-3C, the orbit improvement can reach 7%. The validation with satellite laser ranging also demonstrates the benefit of the integrated orbit determination. Such a high-quality orbit will potentially benefit meteorological studies and applications.

1. Introduction

For the purpose of global climate monitoring and numerical weather prediction, the FengYun-3C (FY-3C) satellite, developed by the Meteorological Administration/National Satellite Meteorological Center of China, was launched on 23 September 2013, with an inclination of 98.75° and a height of 836 km (Yang et al., 2012). For scientific and remote sensing missions, such as Gravity Recovery and Climate Experiment (GRACE) and Jason-1, the precise orbit plays a crucial role in successfully achieving its designed goals. For the purpose of the precise orbit determination (POD) and Global Navigation Satellite Systems (GNSS) radio occultation, FY-3C is equipped with a state-of-the-art receiver, the GNSS Occultation Sounder (GNOS) instrument. Apart from GPS signals, GNOS has the capacity to receive signal from the BDS constellation, which consists of five Geostationary Earth Orbit (GEO) satellites, six Inclined Geosynchronous Satellite Orbit (IGSO) satellites, and three Medium Earth Orbit (MEO) satellites at present. There are three sets of antennas, the rising occultation antenna, the positioning antenna, and the setting occultation antenna installed on GNOS (Bai et al., 2014). Up to six BDS satellites and more than eight GPS satellites can be observed simultaneously through the positioning antenna by GNOS. The onboard FY-3C data have already been successfully used for ionospheric electron density sounding (Mao et al., 2016), atmospheric parameter retrieval (Liao et al., 2016), POD (M. Li et al., 2017; Xiong et al., 2017), and enhancing BDS orbits (Zhao et al., 2017).

Since the successful use of GPS-based POD for TOPEX/Poseidon satellite (Tapley et al., 1994), the onboard GPS technique has been employed for many geoscience and remote sensing missions, such as CHAMP, GRACE, Gravity field and steady state Ocean Circulation Explorer, Swarm, and TerraSAR-X, to obtain high precise orbits at centimeter level (Bock et al., 2011; Hackel et al., 2016; Kang et al., 2006; Kuang et al., 2001; van den IJssel et al., 2015). Usually, a *two-step* method is utilized in low earth orbit (LEO) POD. In this method, first, the ground GNSS observations are used to obtain the precise orbits and clocks correction of

GNSS satellites. Then, based on the estimated orbits and clocks of GNSS satellites, the LEO POD is performed using onboard GNSS data. In other words, the orbits and clocks correction of GNSS satellites are held fixed in the subsequent LEO POD. It is obvious that LEO orbit can be easily affected by the quality of GNSS orbits and the errors of ground stations in the two-step method. By contrast, a so-called *one-step* POD, which can also be called integrated POD, was proposed in the earlier time where the orbits of GNSS satellite and LEO are determined in the integrated adjustment by joint processing the ground and onboard data simultaneously. As a dynamic tracking station, a LEO is expected to achieve global tracking coverage for GNSS satellites orbiting at higher altitude. Different from the ground stations, the motion of LEO can improve the observation geometry of GNSS satellites. Furthermore, the strong algebraic correlations between LEO orbit, GNSS orbits, and the ground reference frame will be introduced in the process of integrated POD.

Zhu et al. (2004) first determined the orbits of GPS and LEO in an integrated orbit determination by combining the ground-based GPS data, onboard GPS data, and satellite laser ranging (SLR) data from the CHAMP and GRACE satellites together, and the result indicates significant accuracy improvement of both GPS and LEO satellite orbits. The integrated POD of LEO and GPS was also implemented by Geng et al. (2006), which proves the ability to compensate the weaknesses of both satellite types. Zoulida et al. (2016) carried out a simultaneous determination of GPS satellite orbits as well as Jason-2 orbit, and the resulting GPS orbits show higher quality compared to that of GPS-only solution. Besides, some other works are also performed by many scholars to investigate the performance of the one-step POD method (Boomkamp & Dow, 2005; Feng et al., 2016; König et al., 2005).

The onboard FY-3C data provide us a great opportunity to investigate the integrated orbit determination of FY-3C, BDS, and GPS satellites. In this contribution, we will focus on the integrated orbit determination of FY-3C, BDS, and GPS by combining the tracking data from ground stations and the onboard FY-3C observations. We designed three network schemes to investigate the influence of station distribution on the integrated POD, and four strategies are performed to evaluate the capability of BDS for integrated orbit determination and the benefit of BDS and GPS fusion. Our paper is organized as follows: section 2 addresses the integrated orbit determination method and describes the detailed processing strategies. In section 3, we evaluate the performance of integrated orbit determination by overlap comparison and orbit comparison with international GNSS service (IGS) final products. And the results are subsequently further assessed by SLR validation in section 4. Finally, a summary of the results and corresponding conclusions are presented in section 5.

2. Integrated Orbit Determination and Processing Strategy

2.1. Integrated Orbit Determination

The GNSS pseudorange and carrier phase observations of ground station and LEO can be written as follows:

$$\begin{aligned}
P^s_{g,j} &= \rho^s_{g,j} + c\cdot\left(\delta t_g - \delta t^s\right) + c\left(b_{g,j} - b^s_j\right) + I^s_{g,j} + T^s_g + \varepsilon^s_{g,j}\\
P^s_{\mathrm{leo},j} &= \rho^s_{\mathrm{leo},j} + c\cdot\left(\delta t_{\mathrm{leo}} - \delta t^s\right) + c\left(b_{\mathrm{leo},j} - b^s_j\right) + I^s_{\mathrm{leo},j} + \varepsilon^s_{\mathrm{leo},j}\\
L^s_{g,j} &= \rho^s_{g,j} + c\cdot\left(\delta t_g - \delta t^s\right) + \lambda_j\left(B_{g,j} - B^s_j\right) - I^s_{g,j} + T^s_g + \lambda_j N^s_{g,j} + \omega^s_{g,j}\\
L^s_{\mathrm{leo},j} &= \rho^s_{\mathrm{leo},j} + c\cdot\left(\delta t_{\mathrm{leo}} - \delta t^s\right) + \lambda_j\left(B_{\mathrm{leo},j} - B^s_j\right) - I^s_{\mathrm{leo},j} + \lambda_j N^s_{\mathrm{leo},j} + \omega^s_{\mathrm{leo},j}
\end{aligned} \tag{1}$$

where subscript g and leo represent the ground station and LEO, respectively. The indices s and j refer to satellite and frequency. $\rho^s_{g,j}$ is the distance between satellite and the ground receiver, while $\rho^s_{\mathrm{leo},j}$ is the distance between satellite and LEO antenna phase centers in meters. c is the speed of light in vacuum. δt_g, δt_{leo}, and δt^s denote the clock offsets of ground station, LEO, and satellite, respectively. λ_j is the wavelength at the frequency j. $b_{g,j}$, $b_{\mathrm{leo},j}$, and b^s_j represent the code bias of ground receiver, onboard receiver, and satellite, respectively. $B_{g,j}$, $B_{\mathrm{leo},j}$, and B^s_j are phase delays of ground receiver, onboard receiver, and satellite, respectively. $I^s_{g,j}$ and $I^s_{leo,j}$ are slant ionospheric delay along the line of sight for ground station and LEO at frequency j. T^s_g is the

slant tropospheric delay of ground station g. Since LEO usually is well above the troposphere, GNSS observations of LEO are not affected by the troposphere, and tropospheric delay terms for LEO can be neglected. $N^s_{g,j}$ and $N^s_{leo,j}$ are the integer ambiguities for ground and onboard receivers, respectively. $\varepsilon^s_{g,j}$ and $\omega^s_{g,j}$ denote the sum of multipath error and observation noise for code and carrier phase observations of ground station, while $\varepsilon^s_{\mathrm{leo},j}$ and $\omega^s_{\mathrm{leo},j}$ are the combination of multipath error and observation noise for code and carrier phase observations of LEO, respectively.

Usually, the ionosphere-free (IF) combination is formed to eliminate the first order of ionospheric delay in POD process. Based on the raw observation in (1), we can formulate IF combination as below:

$$\begin{aligned}
P^s_{g,\mathrm{IF}} &= \rho^s_{g,\mathrm{IF}} + c\cdot\left(\delta t_g - \delta t^s\right) + c\cdot\left(b_{g,\mathrm{IF}} - b^s_{\mathrm{IF}}\right) + T^s_g + \varepsilon^s_{g,\mathrm{IF}} \\
P^s_{\mathrm{leo,IF}} &= \rho^s_{\mathrm{leo,IF}} + c\cdot(\delta t_{\mathrm{leo}} - \delta t^s) + c\cdot\left(b_{\mathrm{leo,IF}} - b^s_{\mathrm{IF}}\right) + \varepsilon^s_{\mathrm{leo,IF}} \\
L^s_{g,\mathrm{IF}} &= \rho^s_{g,\mathrm{IF}} + c\cdot\left(\delta t_g - \delta t^s\right) + \lambda_{\mathrm{IF}}\cdot\left(B_{g,\mathrm{IF}} - B^s_{\mathrm{IF}}\right) + T^s_g + \lambda_{\mathrm{IF}}N^s_{g,\mathrm{IF}} + \omega^s_{g,\mathrm{IF}} \\
L^s_{\mathrm{leo,IF}} &= \rho^s_{\mathrm{leo,IF}} + c\cdot(\delta t_{\mathrm{leo}} - \delta t^s) + \lambda_{\mathrm{IF}}\cdot\left(B_{\mathrm{leo,IF}} - B^s_{\mathrm{IF}}\right) + \lambda_{\mathrm{IF}}N^s_{\mathrm{leo,IF}} + \omega^s_{\mathrm{leo,IF}}
\end{aligned} \tag{2}$$

For ground stations, the coordinates are usually fixed as known values or tightly constrained in the process of integrated POD. An a priori model is usually utilized to correct the dry part of tropospheric delay, and the wet component can be estimated as piecewise constant parameters in the POD procedure. After linearization, the observation equation can be rewritten as

$$\begin{aligned}
p^s_{g,\mathrm{IF}} &= e^s_g\cdot\varphi(t,t_0)^s O^s_0 + c\cdot\left(\delta t_g - \delta t^s\right) + Z^s_{g,\mathrm{Tro}} + c\cdot\left(b_{g,\mathrm{IF}} - b^s_{\mathrm{IF}}\right) + \varepsilon^s_{g,\mathrm{IF}} \\
p^s_{\mathrm{leo,IF}} &= e^s_{\mathrm{leo}}\cdot\varphi(t,t_0)^s O^s_0 - e^s_{\mathrm{leo}}\cdot\varphi(t,t_0)_{\mathrm{leo}} O_{\mathrm{leo},0} + c\cdot(\delta t_{\mathrm{leo}} - \delta t^s) + c\cdot\left(b_{\mathrm{leo,IF}} - b^s_{\mathrm{IF}}\right) + \varepsilon^s_{\mathrm{leo,IF}} \\
l^s_{g,\mathrm{IF}} &= e^s_g\cdot\varphi(t,t_0)^s O^s_0 + c\cdot\left(\delta t_g - \delta t^s\right) + Z^s_{g,\mathrm{Tro}} + \lambda_{\mathrm{IF}}\cdot\left(B_{g,\mathrm{IF}} - B^s_{\mathrm{IF}} + N^s_{g,\mathrm{IF}}\right) + \omega^s_{g,\mathrm{IF}} \\
l^s_{\mathrm{leo,IF}} &= e^s_{\mathrm{leo}}\cdot\varphi(t,t_0)^s O^s_0 - e^s_{\mathrm{leo}}\cdot\varphi(t,t_0)_{\mathrm{leo}} O_{\mathrm{leo},0} + c\cdot(\delta t_{\mathrm{leo}} - \delta t^s) + \lambda_{\mathrm{IF}}\cdot\left(B_{\mathrm{leo,IF}} - B^s_{\mathrm{IF}} + N^s_{\mathrm{leo,IF}}\right) + \omega^s_{\mathrm{leo,IF}}
\end{aligned} \tag{3}$$

$$Z^s_{g,\mathrm{Tro}} = M^s_g\cdot Z_g + m^s_g\cdot(G_{\mathrm{ns}}\cdot\cos a + G_{\mathrm{ew}}\cdot\sin a) \tag{4}$$

$$O^s_0 = \left(x^s_0, y^s_0, z^s_0, v^s_x, v^s_y, v^s_z, p^s_1, p^s_2, \cdots, p^s_n\right)^T \tag{5}$$

$$O_{\mathrm{leo},0} = \left(x_{\mathrm{leo},0}, y_{\mathrm{leo},0}, z_{\mathrm{leo},0}, v_{\mathrm{leo},x}, v_{\mathrm{leo},y,}, v_{\mathrm{leo},z}, p_{\mathrm{leo},1}, p_{\mathrm{leo},2}, \cdots, p_{\mathrm{leo},n}\right)^T \tag{6}$$

where $p^s_{g,\mathrm{IF}}$, $p^s_{\mathrm{leo,IF}}$, $l^s_{g,\mathrm{IF}}$, $l^s_{\mathrm{leo,IF}}$ are *observed minus computed* IF code and phase observation for ground station and LEO, respectively. e^s_g is the unit vector of the direction from the ground station to the satellite, while e^s_{leo} is the unit vector of the direction from LEO to the satellite. $\varphi(t,t_0)^s$ and $\varphi(t,t_0)_{\mathrm{leo}}$ denote the state transition matrix for satellite and LEO from initial epoch t_0 to epoch t. O^s_0 represents the initial state of the satellite, which consists of the position (x^s_0, y^s_0, z^s_0) and velocity (v^s_x, v^s_y, v^s_z) of the satellite at reference epoch t_0, and solar radiation pressure parameters $p^s_1, p^s_2, \cdots, p^s_n$. Likewise, $O_{\mathrm{leo},\,0}$ indicates the LEO initial state and ($x_{\mathrm{leo},\,0}$, $y_{\mathrm{leo},\,0}$, $z_{\mathrm{leo},\,0}$), ($v_{\mathrm{leo},\,x}$, $v_{\mathrm{leo},\,y,}$, $v_{\mathrm{leo},\,z}$), and ($p_{\mathrm{leo},\,1}$, $p_{\mathrm{leo},\,2}$, $\cdots$, $p_{\mathrm{leo},\,n}$) denote the initial position, initial velocity, and force model parameters for LEO, respectively. $Z^s_{g,\mathrm{Tro}}$ is estimated tropospheric parameter for ground station g. Z_g represents the zenith delay of wet component. G_{ns} and G_{ew} represent the north-south (NS) and east-west (EW) delay gradient contributions, respectively. $M^s_g$is the nonhydrostatic mapping function, while m^s_g is the mapping function for the gradient part. a is the azimuth of the line of sight of the individual observation (X. Li et al., 2015). The other symbols have similar meaning as above but for the IF linear combination.

In our study, pseudorange and carrier phase observations on frequencies L1 and L2 for GPS, B1, and B2 for BDS are used to form the IF combination of GPS and BDS. In the case of combined GPS and Beidou (GC combination) POD, the linearized observation equation (3) can be formulated as

$$\begin{cases} p^G_{g,\mathrm{IF}} = e^G_g \cdot \varphi(t,t_0)^G O^G_0 + c\cdot(\delta t_g - \delta t^G) + Z^s_{g,\mathrm{Tro}} + c\cdot\left(b^G_{g,\mathrm{IF}} - b^G_{\mathrm{IF}}\right) + \varepsilon^G_{g,\mathrm{IF}} \\ p^C_{g,\mathrm{IF}} = e^C_g \cdot \varphi(t,t_0)^C O^C_0 + c\cdot(\delta t_g - \delta t^C) + Z^s_{g,\mathrm{Tro}} + c\cdot\left(b^C_{g,\mathrm{IF}} - b^C_{\mathrm{IF}}\right) + \varepsilon^C_{g,\mathrm{IF}} \\ p^G_{\mathrm{leo,IF}} = e^G_{\mathrm{leo}} \cdot \varphi(t,t_0)^G O^G_0 - e^G_{\mathrm{leo}} \cdot \varphi(t,t_0)_{\mathrm{leo}} O_{\mathrm{leo},0} + c\cdot(\delta t_{\mathrm{leo}} - \delta t^G) + c\cdot\left(b^G_{\mathrm{leo,IF}} - b^G_{\mathrm{IF}}\right) + \varepsilon^G_{\mathrm{leo,IF}} \\ p^C_{\mathrm{leo,IF}} = e^C_{\mathrm{leo}} \cdot \varphi(t,t_0)^C O^C_0 - e^C_{\mathrm{leo}} \cdot \varphi(t,t_0)_{\mathrm{leo}} O_{\mathrm{leo},0} + c\cdot(\delta t_{\mathrm{leo}} - \delta t^C) + c\cdot\left(b^C_{\mathrm{leo,IF}} - b^C_{\mathrm{IF}}\right) + \varepsilon^C_{\mathrm{leo,IF}} \\ l^G_{g,\mathrm{IF}} = e^G_g \cdot \varphi(t,t_0)^G O^G_0 + c\cdot(\delta t_g - \delta t^G) + Z^s_{g,\mathrm{Tro}} + \lambda_{G,\mathrm{IF}}\cdot\left(B^G_{g,\mathrm{IF}} - B^G_{\mathrm{IF}} + N^G_{g,\mathrm{IF}}\right) + \omega^G_{g,\mathrm{IF}} \\ l^C_{g,\mathrm{IF}} = e^C_g \cdot \varphi(t,t_0)^C O^C_0 + c\cdot(\delta t_g - \delta t^C) + Z^s_{g,\mathrm{Tro}} + \lambda_{C,\mathrm{IF}}\cdot\left(B^C_{g,\mathrm{IF}} - B^C_{\mathrm{IF}} + N^C_{g,\mathrm{IF}}\right) + \omega^C_{g,\mathrm{IF}} \\ l^G_{\mathrm{leo,IF}} = e^G_{\mathrm{leo}} \cdot \varphi(t,t_0)^G O^G_0 - e^G_{\mathrm{leo}} \cdot \varphi(t,t_0)_{\mathrm{leo}} O_{\mathrm{leo},0} + c\cdot(\delta t_{\mathrm{leo}} - \delta t^G) + \lambda_{G,\mathrm{IF}}\cdot\left(B^G_{\mathrm{leo,IF}} - B^G_{\mathrm{IF}} + N^G_{\mathrm{leo,IF}}\right) + \omega^G_{\mathrm{leo,IF}} \\ l^C_{\mathrm{leo,IF}} = e^C_{\mathrm{leo}} \cdot \varphi(t,t_0)^C O^C_0 - e^C_{\mathrm{leo}} \cdot \varphi(t,t_0)_{\mathrm{leo}} O_{\mathrm{leo},0} + c\cdot(\delta t_{\mathrm{leo}} - \delta t^C) + \lambda_{C,\mathrm{IF}}\cdot\left(B^C_{\mathrm{leo,IF}} - B^C_{\mathrm{IF}} + N^C_{\mathrm{leo,IF}}\right) + \omega^C_{\mathrm{leo,IF}} \end{cases} \tag{7}$$

where the indices *C* and *G* refer to the BDS and GPS satellite, respectively. Note that the code biases ($b^G_{g,\mathrm{IF}}$, $b^C_{g,\mathrm{IF}}$ or $b^G_{\mathrm{leo,IF}}$, $b^C_{\mathrm{leo,IF}}$) in one multi-GNSS receiver are different from each other due to the differences in the signal structure and frequencies of individual GNSS constellation. The differences between these code biases are called intersystem biases (*ISB*). In the GC combined integrated POD, GPS is selected as reference and the code bias for GPS of each station is set to 0, and the *ISB* parameter ($b^C_{g,\mathrm{IF}} - b^G_{g,\mathrm{IF}}orb^C_{\mathrm{leo,IF}} - b^G_{\mathrm{leo,IF}}$) for BDS is introduced subsequently. The code biases of satellites are usually assimilated by satellite clock offset. The phase delays $B_{g,\ \mathrm{IF}}$ and B^s_{IF} will be absorbed by phase ambiguities parameters. Therefore, the estimated parameter can be described as

$$X = \left(O^s_0, O_{\mathrm{leo},0}, \delta\tau_g, \delta\tau_{\mathrm{leo}}, \delta\tau^s, Z^s_{g,\mathrm{Tro}}, n^s_g, n^s_{\mathrm{leo}}, ISB^C_g, ISB^C_{\mathrm{leo}}\right)^T \tag{8}$$

$$\begin{cases} \delta\tau_g = \delta t_g + b^G_{g,\mathrm{IF}} \\ \delta\tau_{\mathrm{leo}} = \delta t_{\mathrm{leo}} + b^G_{\mathrm{leo,IF}} \\ \delta\tau^s = \delta t^s + b^s_{\mathrm{IF}} \end{cases} \tag{9}$$

$$\begin{cases} n^s_g = N^s_g + B_{g,\mathrm{IF}} - B^s_{\mathrm{IF}} \\ n^s_{\mathrm{leo}} = N^s_{\mathrm{leo}} + B_{\mathrm{leo,IF}} - B^s_{\mathrm{IF}} \end{cases} \tag{10}$$

$$\begin{cases} ISB^C_g = b^C_{g,\mathrm{IF}} - b^G_{g,\mathrm{IF}} \\ ISB^C_{\mathrm{leo}} = b^C_{\mathrm{leo,IF}} - b^G_{\mathrm{leo,IF}} \end{cases} \tag{11}$$

All the unknown parameters are estimated in a batch-processing mode based on the ground and onboard observations.

2.2. Processing Strategy

In order to evaluate the performance of integrated orbit modeling for BDS, GPS, and LEO, the ground observations and FY-3C onboard data from day of year (DOY) 321 to DOY 350 in 2013, DOY 081 to DOY 110 in 2015, and DOY 081 to DOY 110 in 2017 are utilized. Three station schemes (see Figure 1), a regional network with 10 multi-GNSS Experiment (MGEX; Montenbruck et al., 2017) ground stations (regional network [RN] scheme), a global network with 34 MGEX ground stations (GN30 scheme), and a global network with 85 MGEX ground stations (GN85 scheme) are designed to investigate the impact of the quantity and distribution of ground stations on integrated POD. In each scheme, we perform BDS, GPS, GC, and GC (without GEO) POD with and without LEO, respectively.

Table 1 lists the BDS, GPS, and FY-3C integrated POD strategy in detail. To make full use of onboard data, the data interval is set to 30 s. We select an arc length of 3 days, which has 48-hr overlapping orbit between two adjacent consecutive orbit arcs. The cutoff elevation angle is set to 7° for ground station and 1° for FY-3C. The

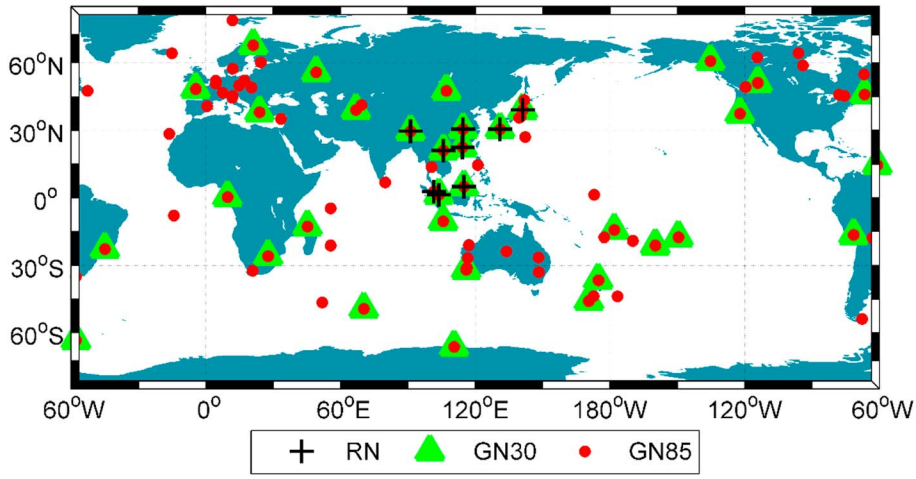

Figure 1. Distribution of the regional and global networks.

GPS phase center offset (PCO) and phase center variation (PCV) corrections from IGS *igs08.atx* model (Schmid et al., 2016) are used, while the PCO values provided by European Space Agency are employed for BDS. Note that the BDS PCV is ignored here. The PCO corrections used for FY-3C are the same as used by M. Li et al. (2017), while the PCV for FY-3C is ignored. The double-difference ambiguity resolution is employed to recover integer property of the ambiguities for the ground network, while the FY-3C ambiguities are estimated as float constant values for each continuous arc, not fixed to integers.

It should be noted that there are some differences between the dynamic model of navigation satellites and FY-3C. The Earth gravity field, one of the main conservative forces, is modeled by EIGEN6C (Förste et al., 2011) up to order and degree 12 for navigation satellites, whereas due to the lower orbit, a higher order gravity field model should be used for LEO. A 120 × 120 EIGEN6C model is employed for LEO to describe the gravity field more elaborately. As for nonconservative forces, main dynamic model differences exist in solar radiation pressure and atmospheric drag. In our study, BDS/GPS satellites utilize the five-parameter ECOM model (Beutler et al., 1994) to describe the solar radiation pressure, and five independent parameters are estimated as arc constants. The solar radiation pressure of FY-3C is computed based on box-wing model with simplified geometric model and panel information of FY-3C. In terms of atmospheric drag, it is usually ignored for navigation satellites because of the thinner atmosphere on the orbit height of BDS/GPS satellites. Differently, the atmosphere drag must be taken into account for LEO. Based on the geometric information about FY-3C, atmospheric drag can be obtained with the atmosphere density computed by DTM94 (Berger et al., 1998) and additionally the drag scale coefficient is estimated as piecewise constant parameter to compensate for the error due to the simplified geometric model. Besides, in order to compensate the unmodeled force errors of LEO, empirical accelerations for LEO in along-track, cross-track, and radial components are estimated as piecewise constant parameters.

3. Results

The integrated POD is performed using onboard FY-3C data and ground observations from regional and global networks during DOY 081–110 in 2017. The arc length we select is 3 days, shifted by 1 day for any two adjacent arcs. In this study, we compare the middle day of one 3-day arc with the first day of the following 3-day arc to exclude the arc boundary degradations. In other words, the 24-hr orbit overlap differences (OODs) are analyzed.

3.1. Integrated POD With Regional Network

BDS and GPS observations of 10 stations in the Asia-Pacific region from MGEX are used in the RN scheme. With regional network, four POD schemes, namely GPS, BDS, GC, and GC (without GEO), are processed with and without LEO, respectively. Figure 2 illustrates the overlap differences of GPS POD with regional network in the along-track, cross-track, radial, and 3-D directions. The 3-D root-mean-square (RMS) of overlap

Table 1
Processing Strategy for the Integrated POD of FY-3C, BDS, and GPS

Model	Description
Observation model	
Observation	Undifferenced ionosphere-free code and phase
Interval	30 s
POD arc length	3 days
Elevation cutoff angle	7° for ground station and 1° for LEO
GNSS PCO and PCV	GPS: the PCO and PCV model from igs08.atx BDS: the PCO model from ESA, PCV not considered
FY-3C PCO and PCV	Use default value to correct PCO, and PCV is not considered
Dynamics model	
Earth gravity	EIGEN6C (12 × 12) for GPS/BDS and EIGEN6C (120 × 120) for FY-3C
N-body	JPL DE405
Ocean tide	FES 2004
Relativity	IERS 2003
Solid tide and pole tide	IERS 2003
Earth radiation pressure	Not considered
Solar radiation pressure	ECOM model for GPS/BDS and box-wing model for FY-3C
Atmospheric density	DTM94, only considered for FY-3C
Empirical accelerations	Only considered for FY-3C, piecewise constant at 90-min intervals
GPS/BDS estimated parameters	
Satellite initial state	Position and velocity at initial epoch
Solar radiation pressure	Five ECOM SRP parameters
Satellite clock offset	Each epoch as white noise
FY-3C estimated parameters	
Satellite initial state	Position and velocity at initial epoch
Atmospheric drag	One constant scale parameter per 360 min
Empirical accelerations	One constant set per 90 min
Receiver clock error	Each epoch as white noise
Ambiguities	Estimated as float constant values for each continuous arc
Intersystem bias	Estimated only for dual-system POD
Ground station estimated parameters	
Station coordinate	Constraint based on SINEX
Zenith wet delay	One constant set per 120 min
Troposphere gradient	One constant set per 1,440 min
Receiver clock error	Each epoch as white noise
Ambiguities	Each continuous arc; double-difference ambiguity resolution for the ground network
Intersystem bias	Estimated only for dual-system POD
ERP parameters	Estimated only for the global network; one set per arc
Estimator	
LSQ	Batch-processing mode

Note. FY-3C = FengYun-3C; POD = precise orbit determination; LEO = low Earth orbit; GNSS = Global Navigation Satellite Systems; ESA = European Space Agency; PCO=phase center offset; PCV=phase center variation; SRP=solar radiation pressure; ERP= earth rotation parameters; LSQ= least square; SINEX= solution independent exchange.

differences is computed as the square root of quadratic sum of RMS values in the three components, which represents the length of the difference vector. All the GPS satellite orbits get an improvement after FY-3C is involved. The average RMS of GPS OODs for the one-step solution is improved by 45%, 49%, and 41% in the along-track, cross-track, and radial components, respectively. Figure 3 shows the time series of daily OOD RMS for FY-3C GPS POD. The average RMS of FY-3C OOD in the along-track, cross-track, and radial components is, respectively, 14.0, 6.3, and 10.9 cm. As expected, the one-step solution for FY-3C shows a better precision than the two-step solution. The average RMS of the one-step solution is reduced to 7.0 cm in along-track, 3.0 cm in cross-track, and 5.1 cm in radial components. It demonstrates that the orbits of both GPS and LEO can benefit from the integrated POD with regional stations.

Figure 4 presents the overlap differences of BDS POD in all directions. Significant improvement can be observed for all BDS satellites when LEO is involved. For IGSO and MEO, the orbit precision of one-step solution can be improved by (11%, 2%, and 20%) and (11%, 13%, and 19%) in the along-track, cross-track, and radial components, respectively. For GEO, the precision improvement can reach up to 40%, 11%, and 1%

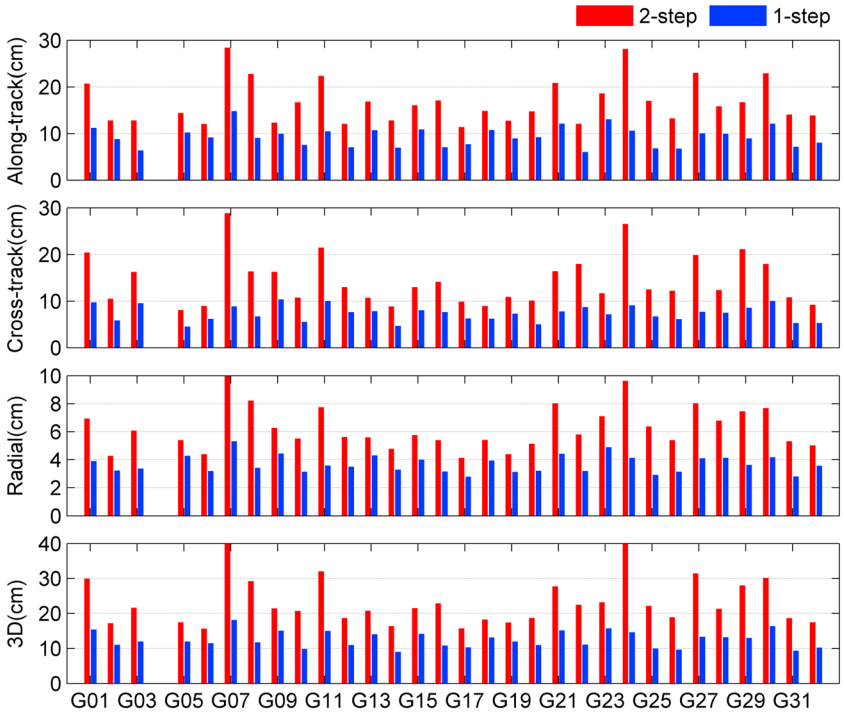

Figure 2. Root-mean-square of orbit overlap differences for GPS precise orbit determination with 10 regional stations. Red and blue bars represent two-step and one-step results, respectively.

in the three components. We can find that the largest precision improvement is achieved for GEO satellites, especially for the along-track component. The main reason is that BDS GEO is almost stationary relative to ground stations, which leads to a static observation geometry. As a moving station, the addition of a LEO

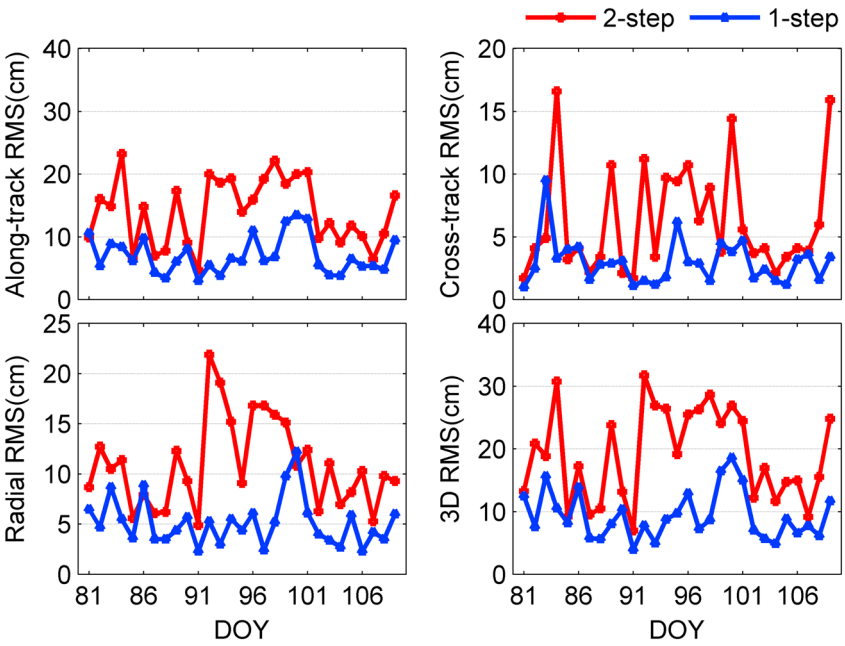

Figure 3. Daily RMS of orbit overlap differences for FengYun-3C GPS precise orbit determination using the two-step and one-step methods with the regional network scheme. Red and blue lines represent two-step and one-step results, respectively. RMS = root-mean-square; DOY = day of year.

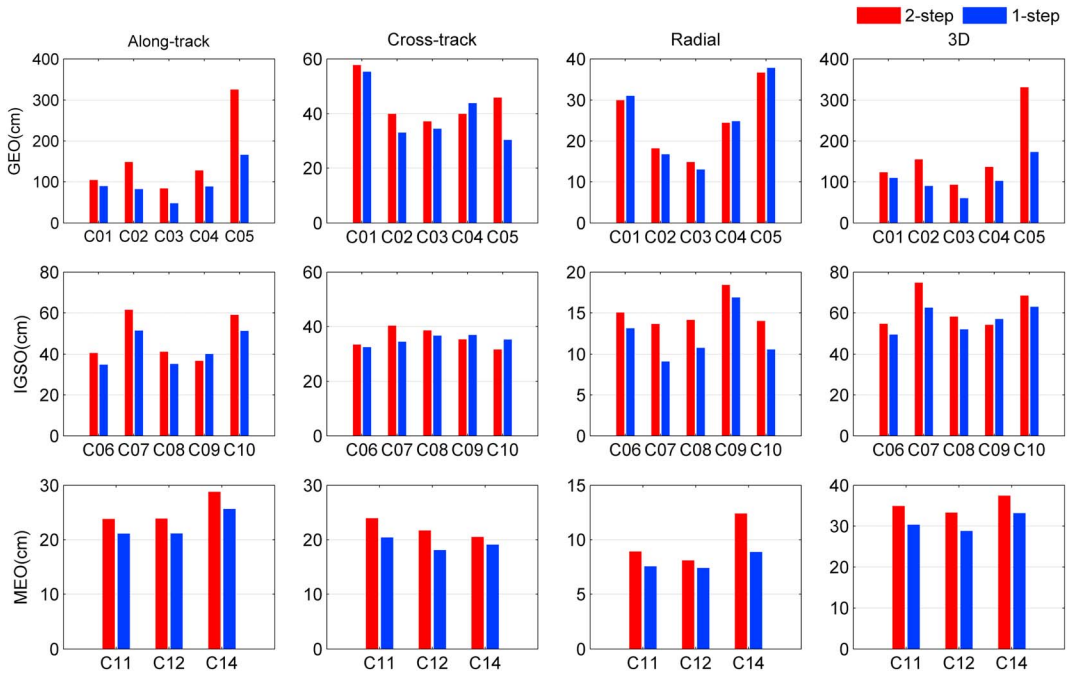

Figure 4. Root-mean-square of orbit overlap differences for BDS precise orbit determination with 10 regional stations. Red and blue bars represent two-step and one-step results, respectively. GEO = Geostationary Earth Orbit; IGSO = Inclined Geosynchronous Satellite Orbit; MEO = Medium Earth Orbit.

can significantly strengthen the observation geometry of GEO. The time series of daily RMS of OODs for FY-3C BDS POD using the two-step and one-step methods are shown in Figure 5. There is an evident improvement in overlap differences for all three components of FY-3C when the integrated POD is processed. Compared with the two-step POD result, the precision of FY-3C orbit for the one-step POD is improved by 71%, 76%, and 75% in the along-track, cross-track, and radial directions, respectively. On the other hand, we can find

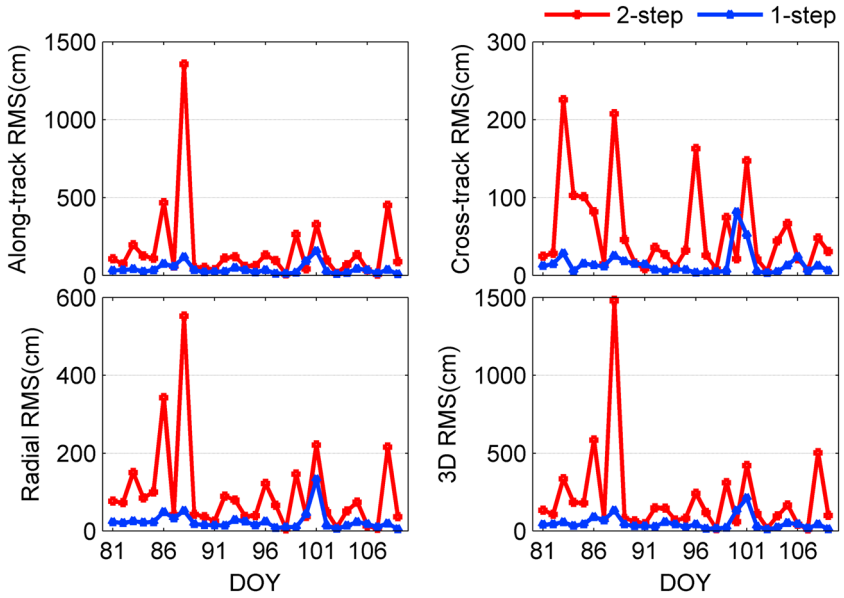

Figure 5. Daily RMS of orbit overlap differences for FengYun-3C BDS precise orbit determination using the two-step and one-step methods with the regional network scheme. Red and blue lines represent two-step and one-step results, respectively. RMS = root-mean-square; DOY = day of year.

Figure 6. Average root-mean-square of GPS and BDS orbit overlap differences for GC combined precise orbit determination with 10 regional stations. GEO = Geostationary Earth Orbit; IGSO = Inclined Geosynchronous Satellite Orbit; MEO = Medium Earth Orbit.

that the FY-3C orbit precision for both the BDS two-step and one-step solutions is much worse than that of the GPS solution, which is due to the few BDS observations of FY-3C.

We implement two GC combined POD schemes with and without GEO, namely, GC and GC (without GEO), to investigate the influence of BDS GEO satellites on GC combined POD using a regional network. Figure 6 shows the RMS of GPS and BDS OODs for the GC combined POD. It can be seen that both GPS and BDS orbits profit from the dual-system combined POD. The average 3-D RMS of GPS, GEO, IGSO, and MEO OODs is 15.4, 142.7, 31.4, and 29.1 cm, respectively, which is better than that of both the single-system

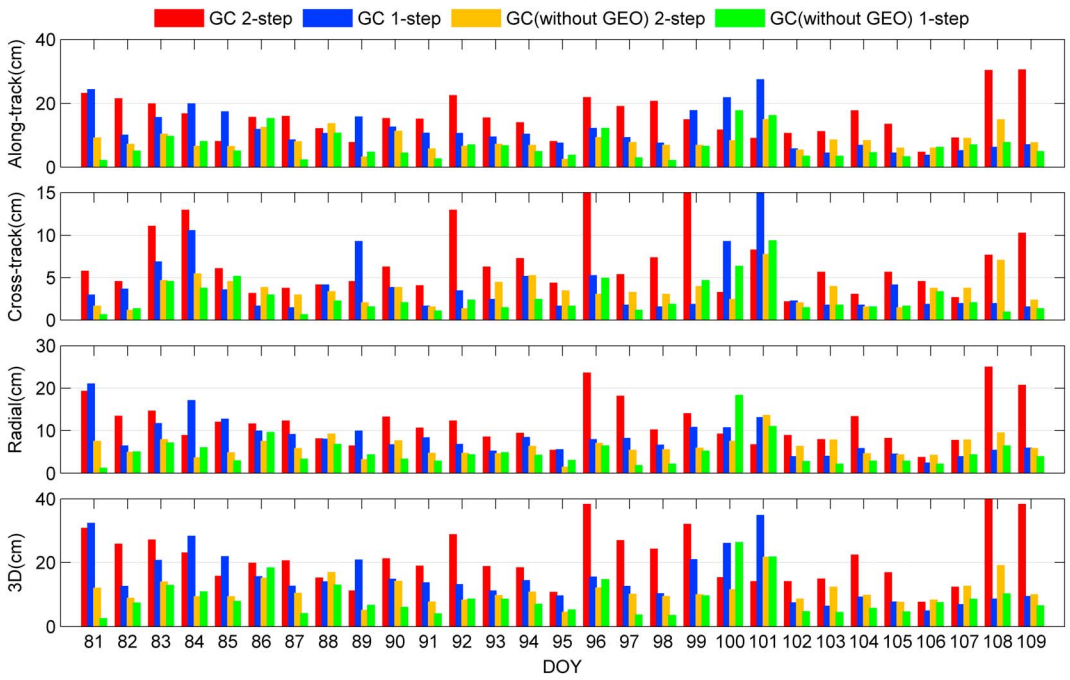

Figure 7. Daily root-mean-square of orbit overlap differences for FengYun-3C GC combined precise orbit determination using the two-step and one-step methods with the regional network scheme. GEO = Geostationary Earth Orbit; DOY = day of year.

solutions (the GPS solution and the BDS solution). It implies that the fusion of GPS and BDS can improve the orbit precision of both constellations with the regional network. This is because the combination of GPS and BDS brings more observations and improves the strength of the POD solution in the case of the regional network. Once the FY-3C onboard data are introduced into the GC POD, the orbit precision of all satellites obtain an obvious improvement. The 3-D RMS of GPS, GEO, IGSO, and MEO OODs is reduced by 20%, 42%, 27%, and 27% when using the one-step method. The largest precision improvement is achieved for GEO, and the improvement in the along-track component plays a dominating role like for the BDS solution.

There is a significant precision improvement for GPS, IGSO, and MEO orbits when BDS GEO satellites are removed from the GC POD process. And GPS, IGSO, and MEO orbits present smaller overlap differences with the 3-D RMS of 12.3, 18.1, and 22.1 cm. This indicates that the inclusion of GEO can result in a significant precision degradation of the estimated orbits. The negative effects of GEO are possibly related to the poor quality of GEO observations, which usually have a severe multipath error from the ground stations due to the geostationary feature of GEO satellites. In addition, the relatively imperfect perturbation models for GEO can also negatively influence the POD. Similar to the GC solution, GPS, IGSO, and MEO orbits for the GC (without GEO) solution achieve a better precision with the FY-3C onboard data involved. Compared with the two-step solution, the orbit precision of GPS, IGSO, and MEO is improved by 24%, 18%, and 36%, respectively.

Figure 7 demonstrates the time series of daily RMS of OOD for FY-3C GC combined POD with the RN scheme. For GC POD, the one-step solution presents a better orbit consistency than the two-step solution. With the one-step method applied, the RMS of FY-3C OOD in the three directions are reduced from (15.9, 7.2, and 11.9 cm) to (11.7, 4.0, and 8.4 cm). It is noteworthy that a few outliers are observed in the GC two-step solution, for example, on DOY 092 and 096, which are not visible in the GC one-step solution. This might indicate that the one-step method allows a more robust detection of outliers. After excluding GEO satellites, FY-3C orbits have smaller overlap differences with OOD RMS of 8.3, 3.5, and 6.3 cm in the three components. An evident precision improvement can be observed for the one-step solution, and the improvement percentage can reach 19%, 23%, and 22% for the along-track, cross-track, and radial directions.

Table 2
The Average 3-D RMS of GPS and BDS Orbit Difference With Respect to the GBM Product

	G		C		GC		GC (without GEO)	
SAT	Two-step	One-step	Two-step	One-step	Two-step	One-step	Two-step	One-step
GPS	23.1	15.0	—	—	15.7	15.0	13.4	11.7
GEO	—	—	722.1	244.1	715.2	234.4	-	-
IGSO	—	—	58.2	52.7	34.7	33.4	29.9	23.5
MEO	—	—	26.2	23.6	23.3	20.2	18.9	14.9

Note. GEO = Geostationary Earth Orbit; IGSO = Inclined Geosynchronous Satellite Orbit; MEO = Medium Earth Orbit; G=GPS; C=BDS; GC=GPS+BDS.

As a reference orbit, the MGEX orbit product can be used as an indicator to evaluate the orbit accuracy of GNSS satellites. In this study, we compare the RN solution with the MGEX final orbit product (GBM) from GeoForschungsZentrum (GFZ) and the RMS of orbit differences are calculated. Table 2 illustrates the 3-D RMS of GPS orbit differences for the GPS, GC, and GC (without GEO) solutions with respect to the GBM product. The results show that for the one-step method, the average 3-D RMS of orbit differences for the GPS, GC, and GC (without GEO) solutions are reduced by 35%, 5%, and 13%, respectively. This indicates that the one-step solution has a better consistency with the MGEX product than the two-step solution. It should be noted that the GC solution presents a smaller RMS than the GPS solution, which means that the fusion of BDS and GPS can improve the POD precision. Table 2 also presents the result of the BDS orbit comparison with respect to the GBM product. Similar to GPS, the orbit differences of BDS for all one-step solutions are smaller than that for the corresponding two-step solutions. Taking the BDS solution as an example, the orbit differences for the one-step solution are reduced by 66% for GEO, 10% for IGSO, and 10% for MEO, respectively. It is noteworthy that, compared to the result of IGSO and MEO satellites, the improvement of orbit precision of GEO satellites is much more evident. This again demonstrates the contribution of onboard BDS GEO data for GEO orbit determination.

3.2. Integrated POD With Global Stations

About 34 globally and evenly distributed stations from the MGEX network are selected for the GN30 scheme. We perform four POD strategies like for the RN scheme to investigate the performance of FY-3C, BDS, and GPS integrated POD with a global network.

Figure 8 presents the overlap differences of individual GPS orbits for GPS POD. On average, the orbit differences for GPS are reduced from 2.4 to 2.2 cm in along-track, from 1.7 to 1.6 cm in cross-track, from 0.9 to 0.8 cm in radial components when the one-step POD are considered. Compared with the RN solution, the GPS orbit for the GN30 one-step solution get a smaller precision improvement. This is mainly because of the larger number of ground stations, thus reducing the contribution of onboard observations from FY-3C in the POD. Table 3 shows the average OOD RMS for FY-3C GPS POD for the GN30 scheme. The precision of FY-3C GPS two-step POD can reach centimeter level. When the integrated orbit determination is implemented, the 3-D RMS of FY-3C OOD is reduced by 11%. This demonstrates that the integrated POD can improve both GPS and LEO orbit precision even with the global network.

The OODs for BDS POD with the GN30 scheme are shown in Figure 9. With the global network, a better orbit precision is achieved for BDS satellites, especially for IGSO and MEO. On average the 3-D RMS of BDS OOD for the two-step solution is 75.4 cm for GEO, 46.8 cm for IGSO, and 14.7 cm for MEO, respectively. Once FY-3C is involved, the orbit precision of BDS satellites can be improved. The improvement percentage of OOD 3-D RMS for GEO, IGSO, and MEO can reach 2%, 6%, and 14%, respectively. Different from the RN solution, BDS GEO orbit of the one-step solution presents the smallest improvement among the three types of BDS satellites. This is reasonable because introducing more global stations can improve the observation geometry for BDS GEO even though the geostationary feature of GEO is not changed, which can weaken the enhancement of onboard observations for GEO. On the other hand, the onboard BDS observations collected by FY-3C are relatively less than GPS observations as the number of tracking channels for BDS is limited, and in addition GEO observations are less than IGSO and MEO observations. These factors also lead to a lower contribution to BDS GEO POD in the case of the global network. Table 3 illustrates the RMS of FY-3C OOD for the BDS POD.

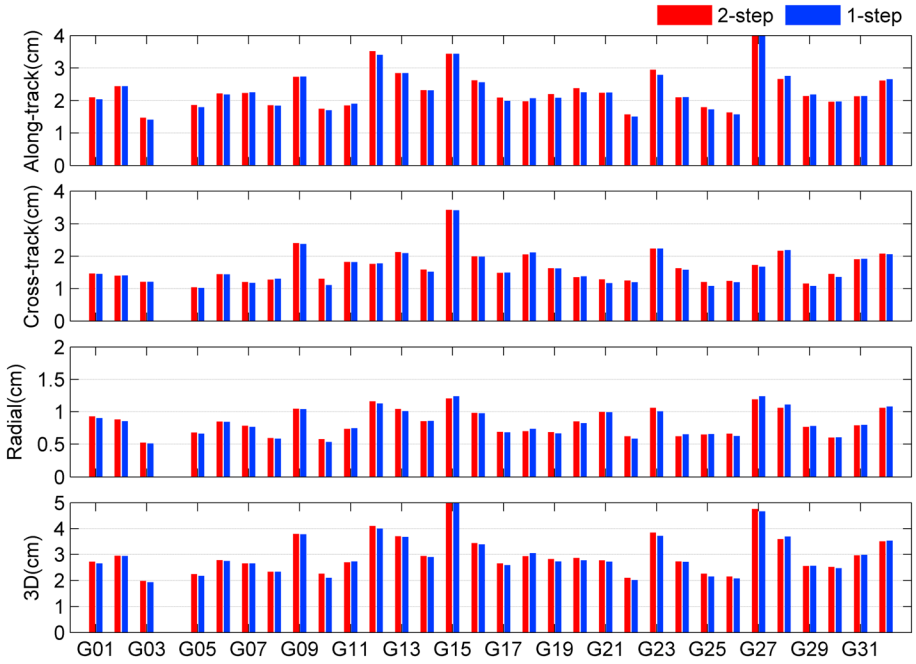

Figure 8. Average root-mean-square of orbit overlap differences for GPS precise orbit determination with 34 global stations. Red and blue bars represent two-step and one-step results, respectively.

The FY-3C OOD for the GN30 solution is much smaller than that for the RN solution owing to the great improvement of BDS orbits and clocks with a global network. Using the one-step method, the FY-3C orbit for the BDS solution achieves a better precision. The OOD RMS for the one-step solution in the along-track, cross-track, and radial components is improved by 30%, 33%, and 33%, respectively.

Figure 10 demonstrates the RMS OOD of GPS and BDS for the GC combined POD using data from global stations. The average 3-D RMS of GPS, GEO, IGSO, and MEO OOD for the two-step solution is 4.5, 71.3, 19.4, and 6.9 cm, respectively. It can be seen that the GPS orbits of the GC combined solutions are worse than that of GPS solution. Different from the RN solution, introducing BDS satellites (particularly BDS GEO) into the POD process with a global network can degrade the GPS orbits. The possible reason is that using the global observations, GPS can already achieve relatively high-precision orbits. In this case, the addition of new constellation with poor-quality observations and relatively improper perturbation models (GEO) will have a slight negative influence on the precision of GPS orbits. After introducing LEO into the POD, the orbit precision of GPS, GEO, IGSO, and MEO is improved by 4%, 5%, 16%, and 19%, respectively.

When BDS GEO satellites are excluded, the 3-D RMS of GPS, IGSO, and MEO OOD is reduced to 3.1, 6.9, and 4.7 cm, respectively. It demonstrates that the inclusion of GEO satellites also have negative effects on the orbits of the other satellites, although more observations from the global network are utilized. With the GC (without GEO) one-step POD performed, GPS, IGSO, and MEO orbits present a better consistency, which

Table 3
Average RMS of FY-3C Orbit Overlap Differences Using the Two-Step and One-Step Methods With the GN30 Scheme (Unit: cm)

	C		G		GC		GC (without GEO)	
Direction	Two-step	One-step	Two-step	One-step	Two-step	One-step	Two-step	One-step
Along	46.1	32.3	1.4	1.3	3.2	3.0	1.6	1.6
Cross	13.5	9.0	0.4	0.5	1.0	1.0	0.4	0.5
Radial	38.1	25.7	1.2	1.0	2.5	2.3	1.3	1.3
3-D	61.3	42.2	1.9	1.7	4.1	3.9	2.1	2.1

Note. FY-3C = FengYun-3C; GEO = Geostationary Earth Orbit; G=GPS; C=BDS; GC=GPS+BDS.

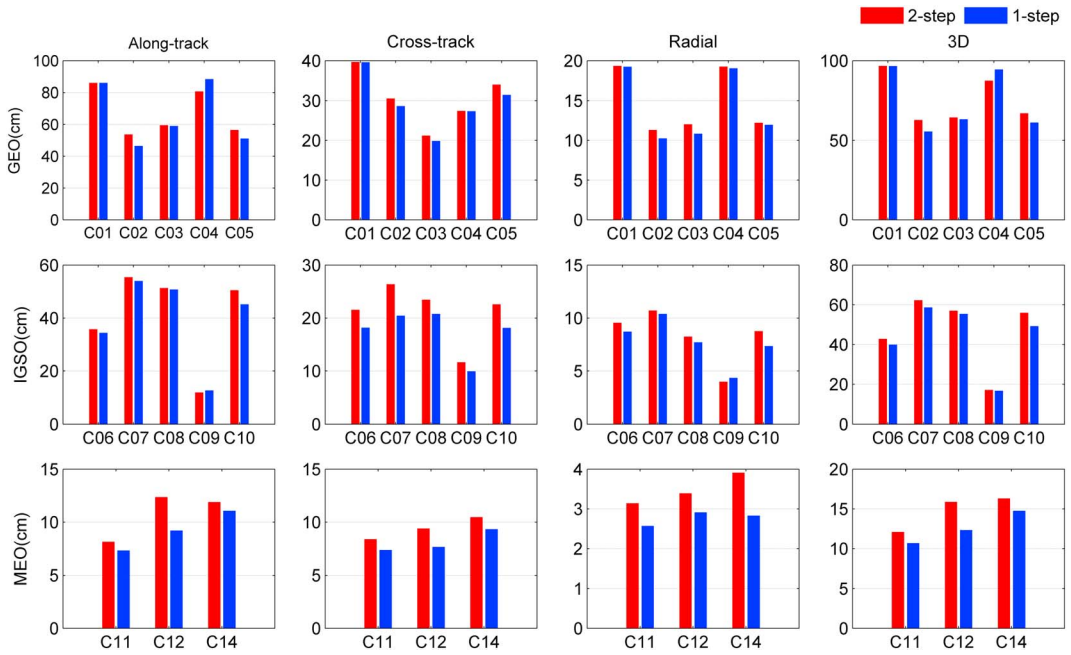

Figure 9. Average root-mean-square of orbit overlap differences for BDS precise orbit determination with 34 global stations. Red and blue bars represent two-step and one-step results, respectively. GEO = Geostationary Earth Orbit; IGSO = Inclined Geosynchronous Satellite Orbit; MEO = Medium Earth Orbit.

are respectively improved by 3%, 7%, and 9% compared to the two-step solution. For FY-3C, the GC combined solution presents a worse consistency than the GPS solution due to the introduction of BDS GEO (see Table 3). An evident improvement can be observed for the GC solution when the one-step approach is used, and the 3-D RMS of FY-3C OOD for the GC one-step solution is reduced by 7%. For the GC (without GEO) POD, the one-step solution almost achieves the same precision as the two-step solution.

To further assess the impact of quantity of ground stations on the integrated POD, approximately 85 tracking stations from MGEX network all over the world are selected in the GN85 scheme from which more than 55 stations have the capacity to track the BDS constellation. These stations are mainly distributed in Europe and a region extending from Australia to East Asia.

Table 4 displays the RMS of GPS, BDS, and FY3C OODs for the GC POD with the GN85 scheme. Compared with the other two schemes (RN and GN30), the inclusion of more ground stations can improve the GPS and BDS orbit precision. Meanwhile, the average RMS of GPS and BDS OOD becomes smaller after onboard data from FY-3C are utilized. Similar to the previous two schemes, the precision improvement of GEO satellites mainly focuses on the along-track component, which can reach 9%. The overlap differences for GPS, IGSO, and MEO are reduced with FY-3C onboard data, which can reach 3% for GPS, 8% for IGSO, and 9% for MEO. In addition, we can see that the orbit of FY-3C GC-combined POD for GN85 solution has a better consistency than that of GN30 solution. The integrated POD can evidently reduce the overlap difference of FY-3C orbit for all three components, which implies the great potential of the integrated POD for improving orbit quality of Earth observing satellites.

3.3. Integrated POD During 2013–2017

In order to access the performance of the integrated POD of BDS, GPS, and FY-3C in different years, we process the observations of global stations and FY-3C from DOY 321–350 in 2013, DOY 081–110 in 2015, and DOY 081–110 in 2017 to perform GPS and GC combined POD, respectively. Note that all the available MGEX stations in 2013 and 2015 are used and the stations from GN85 scheme are used here for 2017.

Figure 11 displays the daily 3-D RMS of GPS OOD in 2013, 2015, and 2017. For GPS-only POD (see the left panel in Figure 11), there is an obvious decreasing trend in overlap difference from 2013 to 2017. The

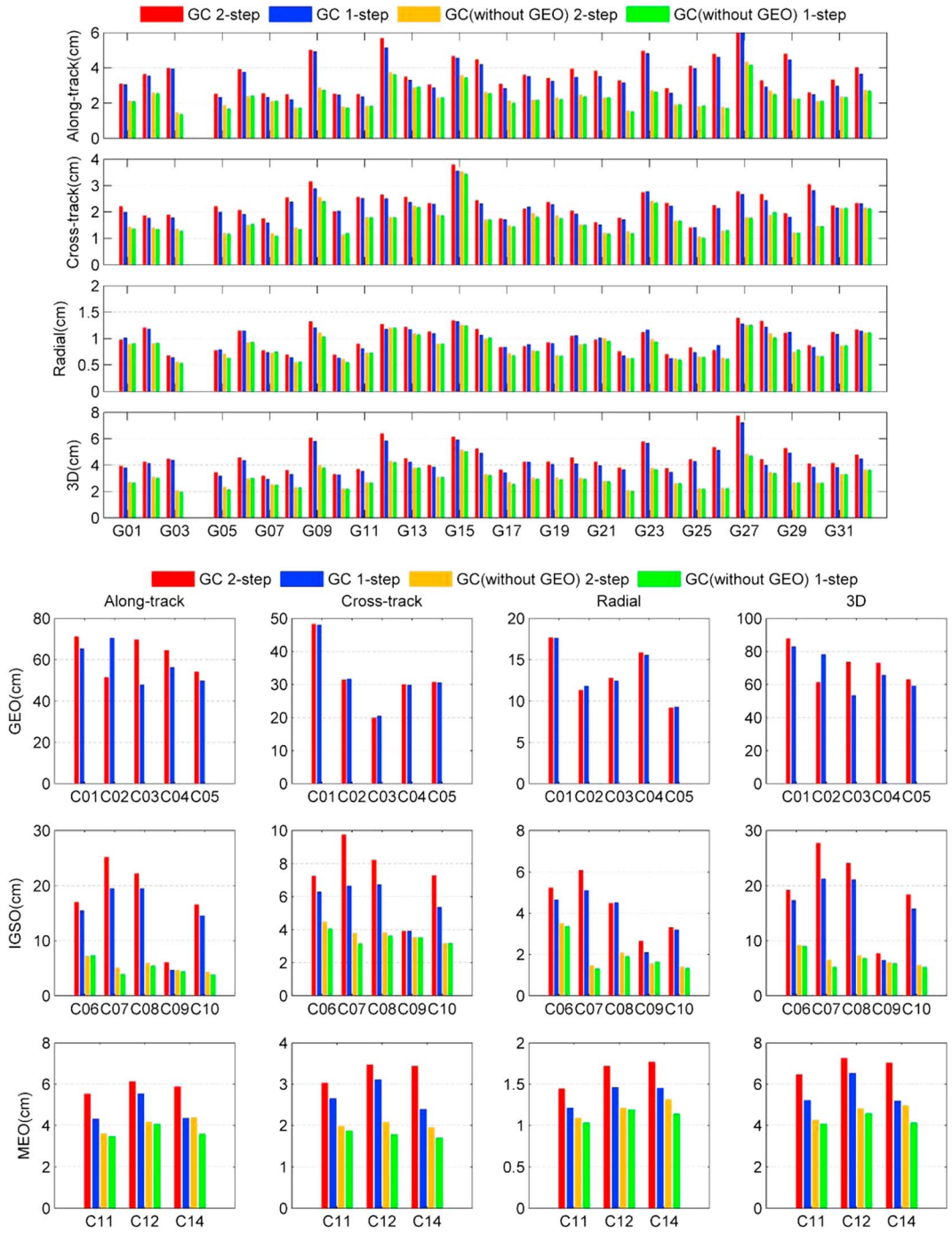

Figure 10. Average root-mean-square of GPS and BDS orbit overlap differences for GC combined precise orbit determination with 34 global stations. GEO = Geostationary Earth Orbit; IGSO = Inclined Geosynchronous Satellite Orbit; MEO = Medium Earth Orbit.

average 3-D RMS of GPS satellites for the two-step solution are 4.9, 4.4, and 3.0 cm, respectively, in 2013, 2015, and 2017. The possible reason is that the number of ground stations used for POD is increasing and that their distribution gets more homogeneous from 2013 to 2017. We can find an orbit precision improvement in 2013, 2015, and 2017 after LEO is involved. The 3-D OOD RMS of the GPS one-step solution are reduced to 4.8, 4.2, and 2.9 cm in 2013, 2015, and 2017, respectively. For the GC POD, the average 3-D RMS of GPS OOD for the two-step solution are 4.0, 4.6, and 3.7 cm, respectively, in 2013, 2015, and 2017. The overlap

Table 4
Average RMS of GPS, BDS, and FY-3C OOD for the GC POD Using the Two-Step and One-Step Methods With the GN85 Scheme (Unit: cm)

	GPS		GEO		IGSO		MEO		FY-3C	
Direction	Two-step	One-step	Two-step	One-step	Two-step	One-step	Two-step	One-step	Two-step	One-step
Along	2.9	2.7	56.1	50.9	13.1	11.9	5.6	5.2	2.9	2.0
Cross	1.9	1.9	28.4	28.5	5.9	5.6	3.1	2.7	0.8	0.5
Radial	1.0	1.0	10.5	10.8	3.5	3.3	1.5	1.5	2.2	1.7
3-D	3.6	3.5	63.7	59.3	14.8	13.6	6.6	6.0	3.7	2.7

Note. FY-3C = FengYun-3C; OOD = orbit overlap differences; POD = precise orbit determination; GEO = Geostationary Earth Orbit; IGSO = Inclined Geosynchronous Satellite Orbit; MEO = Medium Earth Orbit.

differences of GPS orbits for the one-step solution have a smaller RMS than that for the two-step solution in 2017. The average 3-D RMS of GPS satellites for the one-step solution are 4.0, 4.6, and 3.5 cm, respectively, in 2013, 2015, and 2017.

Figure 12 indicates the daily 3-D RMS of BDS satellites OOD for the GC combined POD in 2013, 2015, and 2017. For BDS GEO, notable precision improvement can be easily found in GEO orbit in 2013, 2015, and 2017 when BDS onboard data are used. On average, the overlap differences for GEO have been reduced from 65.0 to 45.7 cm in 2013, 68.9 to 67.5 cm in 2015, and 57.8 to 54.4 cm in 2017. Likewise, the orbit of IGSO for the one-step solution also achieve a better consistency than that of the two-step solution. The IGSO orbit precision for the one-step solution is respectively improved by 8%, 7%, and 7% in the three years. For MEO, no remarkable improvement can be found in 2013 and 2015, while orbit precision is improved slightly by 10% in 2017.

4. SLR Validation

The SLR measurements are only used for an independent validation of BDS satellites orbit since no laser retroreflectors are mounted on FY-3C. In this contribution, the SLR data collected from the International Laser Ranging Service network (Pearlman et al., 2002) are utilized to validate our orbit results. The differences between SLR observations and the computed distance using the BDS orbits and the SLR stations coordinates are calculated. The mean bias and standard deviation (STD) are used as quality indicators. It is noteworthy that the outliers exceeding an absolute value of 1 m for GEO and 0.4 m for IGSO and MEO are excluded from the SLR validation.

Table 5 presents the mean bias and STD of SLR residuals for BDS GEO C01. For the regional solution, both the C and GC one-step solutions have a smaller STD than the two-step solution and it is reduced by 17% for the

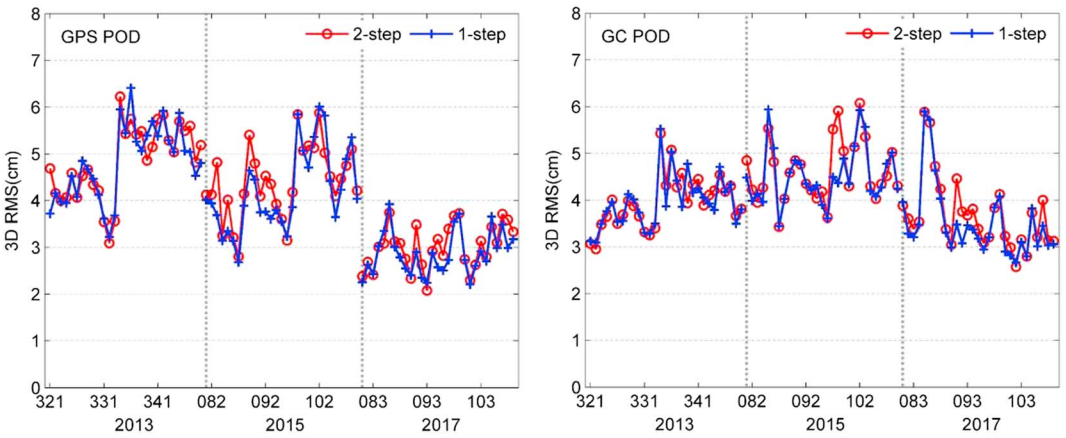

Figure 11. Daily 3-D root-mean-square (RMS) of GPS orbit overlap differences for GPS POD (left panel) and GC POD (right panel) in the years 2013, 2015, and 2017. POD = precise orbit determination.

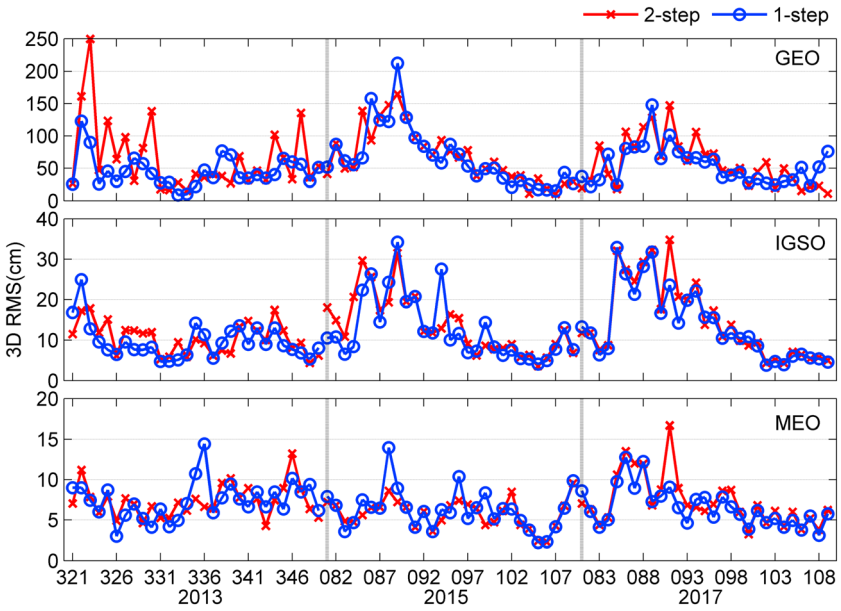

Figure 12. Daily 3-D root-mean-square (RMS) of BDS orbit overlap differences for GC combined precise orbit determination in the years 2013, 2015, and 2017. GEO = Geostationary Earth Orbit; IGSO = Inclined Geosynchronous Satellite Orbit; MEO = Medium Earth Orbit.

BDS solution and 10% for the GC solution when LEO is involved. This is consistent with the previous overlap results in section 3. A similar improvement can also be found in the global solution. Compared to the two-step solution, a smaller STD improvement is achieved by the global one-step solution, which is 5% and 8% for BDS and GC solution, respectively. This is due to the fact that with the increase of the number of ground stations, the contribution of onboard observations from FY-3C is reduced. It is worthwhile to notice that the SLR residuals of BDS C01 has a mean bias of about −40 cm, which may relate to the use of ECOM solar radiation pressure model (Guo et al., 2016). We can find that the SLR bias of the one-step orbit is closer to −40 cm than that of the two-step solution.

Table 6 presents the SLR mean bias and STD for IGSO and MEO satellites. Only the GC (without GEO) solution is analyzed here in order to avoid the precision degradation due to the inclusion of BDS GEOs, which already has been confirmed in section 3. In general, for all solutions, SLR residuals for both IGSO (C08 and C10) and MEO (C11) have an average bias within 3 cm, while the STD are within 3–7 cm. Similar to BDS GEO, the SLR residuals of IGSO and MEO for the regional solution present a smaller variation after the introduction of FY-3C. For the global solution, the SLR STD of the one-step solution is comparable to that of the two-step solution. The SLR STD of C08 (IGSO) for the one-step solution is slightly smaller than that for the two-step solution, while the SLR STD of C11 (MEO) for the one-step solution is slightly larger than that of the two-step solution.

Table 5
Mean Bias and Standard Deviation of C01 (GEO) SLR Residuals for the BDS and GC Solutions (Unit: cm)

		C				GC			
		Two-step		One-step		Two-step		One-step	
Solution	PRN	Mean	STD	Mean	STD	Mean	STD	Mean	STD
RN	C01	−15.3	44.3	−36.8	37.0	−14.7	39.4	−36.7	35.6
GN30	C01	−29.1	21.6	−36.4	20.5	−30.2	17.1	−34.8	15.8

Note. GEO = Geostationary Earth Orbit; SLR = satellite laser ranging; RN = regional network; STD = standard deviation; C=BDS; PRN= pseudo-random noise.

Table 6
Mean Bias and Standard Deviation of SLR Residuals for C08 (IGSO), C10 (IGSO), and C11 (MEO) (Unit: cm)

		GC (without GEO)			
		Two-step		One-step	
Solution	PRN	Mean	STD	Mean	STD
RN	C08	−2.1	5.7	−1.3	5.4
	C10	1.6	6.2	1.6	4.7
	C11	1.9	7.1	2.2	6.6
GN30	C08	−2.0	3.8	−2.1	3.7
	C10	−0.3	3.5	−0.4	3.5
	C11	2.2	4.0	2.3	4.2

Note. SLR = satellite laser ranging; IGSO = Inclined Geosynchronous Satellite Orbit; MEO = Medium Earth Orbit; GEO = Geostationary Earth Orbit; STD = standard deviation; RN = regional network; C=BDS; PRN=pseudo-random noise.

5. Conclusions

In this paper, we developed the integrated orbit determination of FY-3C, BDS, and GPS using onboard FY-3C data along with the regional and global network during 2013–2017. The overlap comparison result shows that the integrated orbit determination can significantly improve the orbit of both FY-3C and navigation satellites. Along with a regional network, the largest orbit improvement is achieved for BDS GEO, especially for the along-track component, and the precision improvement of BDS GEO can reach up to 42% for the GC one-step solution. It is reasonable because introducing LEO as a moving station into the POD can significantly strengthen the observation geometry for GEO with a regional network. Meanwhile, we find that introducing BDS GEO into the POD process can degrade the orbit quality of the other satellites because of the poor quality of GEO observations and the improper perturbation models for GEO.

Using the globally distributed network, GPS, BDS, and FY-3C orbits can get a better precision than that for the regional solution because of more ground stations involved in the POD process. The orbit precision improvement can also be achieved for both FY-3C and navigation satellites when the integrated orbit determination is employed. The improvement of GPS, GEO, IGSO, MEO, and FY-3C orbits can reach 5%, 5%, 16%, 19%, and 7%, respectively. However, the precision improvement of the global one-step solution is smaller than that of the regional solution, because the inclusion of more global stations can weaken the enhancement of LEO for GNSS satellite orbits. More contributions from LEO can be expected as more onboard data are used. Also, the orbit degradation for GPS, IGSO, MEO, and FY-3C due to including BDS GEO can be observed in the global network.

The SLR data collected from the International Laser Ranging Service network are utilized to validate our BDS orbits. For the regional network, the SLR residuals of the one-step solution are smaller than those of the two-step solution. The STD reduction of SLR residuals for the one-step solution is 17%, 5%, 24%, and 7% for BDS C01 (GEO), C08 (IGSO), C10 (IGSO), and C11 (MEO), respectively. Meanwhile, it can be seen that the mean bias for C01 (GEO) is closer to −40 cm, when the one-step method is implemented. With a global network, almost similar SLR STD has been achieved for both the one-step and two-step solutions. The SLR validation results further confirm the benefit of the integrated orbit determination.

These initial results demonstrate the capacity of BDS (with the exception of GEO) for the integrated POD and the potential of integrated orbit determination to improve the orbit of both LEO and navigation satellites. These high-precision orbit products will without a doubt provide important support and guarantee to the atmospheric studies and scientific applications.

Acknowledgments
We are very grateful to the International GNSS Service (IGS) for providing the multi-GNSS data and the precise orbit and clock products of GPS and BDS at the IGS website (ftp://cddis.gsfc.nasa.gov). Also, we greatly appreciate the International Satellite Laser Ranging Service for their continued effort to collect and publicly provide SLR observations. Thanks also go to the EPOS-RT/PANDA software from GFZ. The numerical calculations in this paper have been done on the supercomputing system in the Supercomputing Center of Wuhan University. This study was financially supported by the National Natural Science Foundation of China (grant 41774030).

References

Bai, W., Sun, Y., Du, Q., Yang, G., Yang, Z., Zhang, P., et al. (2014). An introduction to the FY3 GNOS instrument and mountain-top tests. *Atmospheric Measurement Techniques*, *7*(6), 1817–1823. https://doi.org/10.5194/amt-7-1817-2014

Berger, C., Biancale, R., Ill, M., & Barlier, F. (1998). Improvement of the empirical thermospheric model DTM: DTM94-comparative review on various temporal variations and prospects in space geodesy applications. *Journal of Geodesy*, *72*(3), 161–178. https://doi.org/10.1007/s001900050158

Beutler, G., Brockmann, E., Gurtner, W., Hugentobler, U., Mervart, L., Rothacher, M., & Verdun, A. (1994). Extended orbit modeling techniques at the CODE processing center of the international GPS service for geodynamics (IGS): Theory and initial results. *Manuscripta Geodaetica*, *19*, 367–386.

Bock, H., Jäggi, A., Meyer, U., Visser, P., van den Ijssel, J., van Helleputte, T., et al. (2011). GPS-derived orbits for the GOCE satellite. *Journal of Geodesy*, *85*(11), 807–818. https://doi.org/10.1007/s00190-011-0484-9

Boomkamp, H., & Dow, J. (2005). Use of double difference observations in combined orbit solutions for LEO and GPS satellites. *Advances in Space Research*, *36*(3), 382–391. https://doi.org/10.1016/j.asr.2004.12.042

Feng, L., Ruan, R., Wu, X., Sun, B. (2016). Precise orbit determination of navigation satellite using joint data from regional tracking station and LEO. China Satellite Navigation Conference (CSNC) 2016. Changsha, China, 2016

Förste, C., Bruinsma, S., Shako, R., Marty, J-C., Flechtner, F., Abrykosov, O., (2011). EIGEN-6—A new combined global gravity field model including GOCE data from the collaboration of GFZ Potsdam and GRGS Toulouse. (Geophysical Research Abstracts Vol.13, EGU2011–3242-2, 2011), General Assembly European Geosciences Union, Vienna, Austria, 2011

Geng, J., Shi, C., Zhao, Q., Ge, M., & Liu, J. (2006). *Integrated adjustment of LEO and GPS in precision orbit determination*. Wuhan, China: International Association of Geodesy Symposia.

Guo, J., Xu, X., Zhao, Q., & Liu, J. (2016). Precise orbit determination for quad-constellation satellites at Wuhan University: Strategy, result validation, and comparison. *Journal of Geodesy*, *90*(2), 143–159. https://doi.org/10.1007/s00190-015-0862-9

Hackel, S., Montenbruck, O., Steigenberger, P., Balss, U., Gisinger, C., & Eineder, M. (2016). Model improvements and validation of TerraSAR-X precise orbit determination. *Journal of Geodesy*, *91*(5), 1–16.

Kang, Z., Tapley, B., Bettadpur, S., Ries, J., Nagel, P., & Pastor, R. (2006). Precise orbit determination for the GRACE mission using only GPS data. *Journal of Geodesy*, *80*(6), 322–331. https://doi.org/10.1007/s00190-006-0073-5

König, R., Reigber, C., & Zhu, S. (2005). Dynamic model orbits and Earth system parameters from combined GPS and LEO data. *Advances in Space Research*, *36*(3), 431–437. https://doi.org/10.1016/j.asr.2005.03.064

Kuang, D., Bar-Sever, Y., Bertiger, W., Desai, S., Haines, B., Iijima, B., et al. (2001). Precision orbit determination for CHAMP using GPS data from BlackJack receiver. The National Technical Meeting of The Institute of Navigation, Long Beach, American, January 2001.

Li, M., Li, W., Shi, C., Jiang, K., Guo, X., Dai, X., et al. (2017). Precise orbit determination of the Fengyun-3C satellite using onboard GPS and BDS observations. *Journal of Geodesy*, *4*, 1–15.

Li, X., Zus, F., Lu, C., Ning, T., Dick, G., Ge, M., et al. (2015). Retrieving high-resolution tropospheric gradients from multiconstellation GNSS observations. *Geophysical Research Letters*, *42*, 4173–4181. https://doi.org/10.1002/2015GL063856

Liao, M., Zhang, P., Yang, G., Bi, Y., Liu, Y., Bai, W., et al. (2016). Preliminary validation of the refractivity from the new radio occultation sounder GNOS/FY-3C. *Atmospheric Measurement Techniques*, *9*(2), 9009–9044.

Mao, T., Sun, L., Yang, G., Yue, X., Yu, T., Huang, C., et al. (2016). First ionospheric radio-occultation measurements from GNSS occultation sounder on the Chinese Feng-Yun 3C satellite. *IEEE Transactions on Geoscience and Remote Sensing*, *54*(9), 5044–5053. https://doi.org/10.1109/TGRS.2016.2546978

Montenbruck, O., Steigenberger, P., Prange, L., Deng, Z., Zhao, Q., Perosanz, F., et al. (2017). The multi-GNSS Experiment (MGEX) of the International GNSS Service (IGS)—Achievements, prospects and challenges. *Advances in Space Research*, *59*(7), 1671–1697. https://doi.org/10.1016/j.asr.2017.01.011

Pearlman, M., Degnan, J., & Bosworth, J. (2002). The International Laser Ranging Service. *Advances in Space Research*, *30*(2), 135–143. https://doi.org/10.1016/S0273-1177(02)00277-6

Schmid, R., Dach, R., Collilieux, X., Jäggi, A., Schmitz, M., & Dilssner, F. (2016). Absolute IGS antenna phase center model igs08.Atx: Status and potential improvements. *Journal of Geodesy*, *90*(4), 343–364. https://doi.org/10.1007/s00190-015-0876-3

Tapley, B. D., Ries, J., Davis, G., Eanes, R., Schutz, B., Shum, C., et al. (1994). Precision orbit determination for TOPEX/POSEIDON. *Journal of Geophysical Research*, *99*(C12), 24,383–24,404. https://doi.org/10.1029/94JC01645

van den IJssel, J., Encarnação, J., Doornbos, E., & Visser, P. (2015). Precise science orbits for the Swarm satellite constellation. *Advances in Space Research*, *56*(6), 1042–1055. https://doi.org/10.1016/j.asr.2015.06.002

Xiong, C., Lu, C., Zhu, J., & Ding, H. (2017). Orbit determination using real tracking data from FY3C-GNOS. *Advances in Space Research*, *60*(3), 543–556. https://doi.org/10.1016/j.asr.2017.04.013

Yang, J., Zhang, P., Lu, N., Yang, Z., Shi, J., & Dong, C. (2012). Improvements on global meteorological observations from the current Fengyun 3 satellites and beyond. *International Journal of Digital Earth*, *5*(3), 251–265. https://doi.org/10.1080/17538947.2012.658666

Zhao, Q., Wang, C., Guo, J., Yang, G., Liao, M., Ma, H., & Liu, J. (2017). Enhanced orbit determination for BeiDou satellites with FengYun-3C onboard GNSS data. *GPS Solutions*, *21*(3), 1179–1190. https://doi.org/10.1007/s10291-017-0604-y

Zhu, S., Reigber, C., & König, R. (2004). Integrated adjustment of CHAMP, GRACE, and GPS data. *Journal of Geodesy*, *78*(1–2), 103–108.

Zoulida, M., Pollet, A., Coulot, D., Perosanz, F., Loyer, S., Biancale, R., & Rebischung, P. (2016). Multi-technique combination of space geodesy observations: Impact of the Jason-2 satellite on the GPS satellite orbits estimation. *Advances in Space Research*, *58*(7), 1376–1389. https://doi.org/10.1016/j.asr.2016.06.019